European Journal of Sustainable Development Research
2023, 7(2), em0215
e-ISSN: 2542-4742
https://www.ejosdr.com

MODESTUM

Research Article

OPEN ACCESS

Kinetics and thermodynamics investigation of pyrolysis of butyl rubber tube waste

Draksharapu Rammohan [1], Nanda Kishore [1*], Ramgopal V. S. Uppaluri [1]

[1] Department of Chemical Engineering, Indian Institute of Technology Guwahati, Guwahati, Assam, INDIA
***Corresponding Author:** nkishore@iitg.ac.in

Citation: Rammohan, D., Kishore, N., & Uppaluri, R. V. S. (2023). Kinetics and thermodynamics investigation of pyrolysis of butyl rubber tube waste. *European Journal of Sustainable Development Research, 7*(2), em0215. https://doi.org/10.29333/ejosdr/12878

ARTICLE INFO

Received: 18 Oct. 2022

Accepted: 18 Jan. 2023

ABSTRACT

Pyrolysis of butyl rubber tube waste was performed under an inert nitrogen gas environment for temperature ranging between 25 and 1,000 °C, by varying the heating rates (5, 10, 20, 35, and 55 °C min^{-1}). Five different iso-conversional approaches, namely, Differential Friedman, Ozawa-Flynn-Wall, Kissinger-Akahira-Sunuse, Distributed activation, and Starink, were employed to investigate the kinetics and thermodynamic parameters. The mean activation energy (E_α), and pre-exponential factor (k_o) varied between 222.67 and 244.73 kJ mol^{-1} and 6.82×10^{21} and 2.73×10^{24} s^{-1} respectively, for all iso-conversional approaches. From the kinetic investigation, a strong correlation co-efficient (R^2>0.97) was ascertained in the conversion range of up to α=0.8 for all the iso-conversational approaches. By thermodynamic analysis, the mean values of change in enthalpy and change in Gibbs free energy were 217.06-239.13 kJ mol^{-1} and 185.12-218.11, kJ mol^{-1}, respectively. From the master plot analysis, diffusion model (D3), and several reaction order models (F1, F2, F3, and F5) were predicted throughout the conversion (0.1 to 0.8) limit at 20 °C min^{-1} for the pyrolysis of BRT.

Keywords: butyl rubber tube waste, pyrolysis, kinetics, Criado's plot, thermodynamics, activation energy

INTRODUCTION

Energy scarcity and environmental pollution are the two most pressing issues confronting humanity today. This is due to the rapid industrialization, increasing population, and disposal of various solid wastes generated on regular activity. Scientists are developing advanced technologies to recover energy and valuable products from solid waste, including non-biodegradable materials, to address energy scarcity and pollution. Examples of such materials include biomass, municipal, industrial and agricultural solid wastes, and plastics and rubbers.

Rubber is an elastic material classified into diene, (which contains C=C bonds and water) and non-diene (which contains C-C bonds). Diene rubbers are categorized into natural (isoprene) and synthetic (chloroprene, butadiene, styrene-butadiene, and acrylic nitrile-butadiene) rubbers. Non-diene rubbers, such as acrylic, ethylene-propylene, fluorine, urethane, silicone, and butyl, are synthetic rubbers (SRs) (Armada et al., 2022; Shimada et al., 2020; Xu et al., 2020). Butyl rubber is a copolymer of isobutylene (about 98 mass%) and isoprene (about two mass%), which has been utilized for a variety of applications, including automobile parts, cable insulation, gas masks, pharmaceutical stoppers, protective clothing, vibration-dampers, and vehicle inner tubes (EPA, 2020; Nkosi et al., 2021).

Tube and tire waste disposal and management is a significant economic and environmental challenge in the current period of growing globalization (Labaki & Jeguirim, 2017; Nikiema & Asiedu, 2022; Sibeko et al., 2020). Globally, 9.16 MT of vehicle tire waste produced in 2018, and out of that 18.2%, 27.3%, and 54.5%, respectively, have been assessed for energy recovery, combustion, and landfill applications (EPA, 2020). According to a case study conducted by the Energy and Bioproducts Research Institute, the United Kingdom produces between 30.5 and 150 MT of bicycle tire and inner tube waste per year (Taylor, 2020). As a result, empirical evidence on the generation of tire and tube waste must be processed appropriately to recover the maximum amount of additional energy from its massive utility. Thus, an environmentally sustainable mechanism for butyl rubber tube (BRT) waste utilization is required, and pyrolysis is one of the foremost intriguing processes.

Pyrolysis of the tube provides the essential information pertinent to its degradation through kinetic analysis. Most notably, it elucidates the fundamental knowledge about the relevant mechanisms of the reactions and the progression of a mathematical method to demonstrate the process (Huang et al., 2017; Rammohan et al., 2022b). A thorough understanding of the various competent kinetic analysis also helps examine the economic viability of the pyrolytic thermochemical conversion process (Xu et al., 2021; Vo et al., 2017). Thermogravimetric analysis (TGA) is an efficient technique for

performing crucial assessments of kinetics of pyrolysis of BRT waste along with corresponding reaction mechanisms and thermodynamics using model-fitting and model-free iso-conversational techniques (He et al., 2019; Vyazovkin et al., 2011; Yurdakul et al., 2021). The kinetic information collected from these studies is critical for optimizing the thermochemical conversion processes, pyrolizer design and processing parameters. When polymeric material (BRT waste) is subjected to pyrolysis, complicated reaction mechanisms such as primary reactions (chain scission), depolymerization, cyclization, and secondary reactions (cyclic product degradation) take place (Kishore et al., 2003; Lah et al., 2013; Pradhan & Singh, 2015). Several authors had studied the pyrolytic behavior of different types of polymeric materials such as milk packet waste (MPW) by Singh et al. (2019), polyethylene (PE) by Singh et al. (2021), natural rubber (NR) by Danon et al. (2015) and Kordoghli et al. (2017a), Synthetic rubber (SR) by Danon et al. (2015), Khiari et al. (2018), and Kordoghli et al. (2017b), butadiene rubber (BR) by Danon et al. (2015), and styrene-butadiene rubber (SBR) by several researchers (Aboelkheir et al., 2019; Danon et al., 2015; Kawale & Kishore, 2021; Khiari et al., 2018; Kordohhli et al., 2017; Lah et al., 2013; Nkosi et al., 2021; Pradhan & Singh, 2015; Youn et al., 2021).

From the above cited literature, it is obvious that kinetics and thermodynamics of pyrolysis of BRT has not been reported in the open literature. Thus, the current study focuses on the pyrolysis of bicycle inner tubes, such as BRT waste as a feedstock to find its pyrolytic kinetics and thermodynamic properties.

MATERIALS AND APPROACHES

Feed Material Preparation

BRT waste material was gleaned from the backyards of local bicycle puncture repair shops near Indian Institute of Technology Guwahati. The gleaned BRT waste was cut into small particle sizes (<250 µm) with the help of a scissor and then sieved through a BSS 60 mesh. Then after, particles were cleaned with DI water and sundried. Finally, the purified BRT feed material was stored in a glass vial and subjected to further TGA.

Physico-Chemical Characterization

Physicochemical characteristics of BRT waste were determined using ASTM standards. Proximate (volatile: ASTME872-82, moisture: ASTM E1756-08, and ash: ASTM E1755-01) and ultimate analysis (CHNS analyzer: Euro EA 3000), as well as a higher heating value (HHV) (oxygen bomb calorimeter: IS 1350-1, Toshniwal), were included in these characteristics.

Thermogravimetric Analysis

BRT waste pyrolytic decomposition was evaluated using a thermogravimetric analyser (TGA: TG209F1). Non-isothermal TGA experiments were conducted at different heating rates (β) such as 5, 10, 20, 35, and 55 °C min^{-1}. For each experiment, about six mg of sample was taken and subjected temperatures ranging between 25 to 1,000 °C in the TGA, while nitrogen gas at 20 and 40 mL/min was used as protective and carrier gas.

Kinetics Estimation

Estimations of kinetics of pyrolysis of BRT waste were investigated in the present study. Activation energy, E_α (kJ mol^{-1}), and pre-exponential factor, k_o (min^{-1}) were included in the kinetics. These were estimated employing five iso-conversational approaches (model-free, and model fitting), and Criado's master plot approach was utilized for the prediction of model of the reaction (Z_α).

The following general descriptions were given for the pyrolytic decomposition of BRT waste:

$$BRT_{solid} \xrightarrow[T = 25-1{,}000\,^oC;\; N_2 = 40\ mL/min]{k(T)} > Volatiles_{C+NC} + Char_{solid} \quad (1)$$

where C is condensible, and NC is noncondensible.

The conversion rate was, as follows:

$$\frac{d\alpha}{dt} = k(T) f(\alpha) \quad (2)$$

where $f(\alpha)$ is reaction model, $k(T)$ *is* rate constant of the reaction, and $\frac{d\alpha}{dt}$ is conversion rate.

The degree of conversion was expressed, as follows:

$$\alpha = \frac{m_i - m_t}{m_i - m_f} \quad (3)$$

Where m_i, m_f, and m_t were the masses at the beginning (t=0), end (t=end), and any time (t>0), respectively.

The reaction rate was calculated using the Arrhenius equation, as follows:

$$k(T) = k_o exp(-\frac{E_\alpha}{RT}) \quad (4)$$

where T represents absolute temperature (K), E_α represents activation energy (kJ mol^{-1}), R represents universal gas constant (J mol^{-1} K^{-1}), k_o represents pre-exponential factor (min^{-1}), and $k(T)$ represents reaction rate.

Obtain the following from Eq. (2) and Eq. (4):

$$\frac{d\alpha}{dt} = k_o exp\left(-\frac{E_\alpha}{RT}\right) f(\alpha) \quad (5)$$

Now, specify the heating rate (β), as follows:

$$\beta = \frac{dT}{dt} = \frac{dT}{d\alpha} \times \frac{d\alpha}{dt} \quad (6)$$

Obtain the following from Eq. (5) and Eq. (6):

$$g(\alpha) = \int_0^\alpha \frac{d\alpha}{f(\alpha)} = \frac{k_o}{\beta} \int_{T_o}^{T} exp\left(-\frac{E_\alpha}{RT}\right) dT = \frac{k_o E_\alpha}{\beta R} \int_x^\infty u^{-2} exp^{-u} du = \frac{k_o E_\alpha}{\beta R} p(x) \quad (7)$$

where $x = \frac{E_\alpha}{RT}$.

There was no analytical solution to the above integral form of Eq. (7), but it can be solved using several approximation approaches for the solution of E_α and k_o as explained by below approaches.

Differential Friedman approach

The generalized differential Friedman (DFM) (Friedman, 1964) expression was, as follows:

Table 1. Various models in both differential (*f[α]*) and integral form (*g[α]*)

Model	Model code	Differential form $f(\alpha)=\frac{1}{k}\frac{d\alpha}{dt}$	Integral form $g(\alpha)=kt$	$Z(\alpha)=f(\alpha)\times g(\alpha)$
Nucleation model				
Power law	P2	$2(\alpha)^{1/2}$	$(\alpha)^{1/2}$	$2(\alpha)^{1/2}\times(\alpha)^{1/2}$
Power law	P3	$3(\alpha)^{2/3}$	$(\alpha)^{1/3}$	$3(\alpha)^{2/3}\times(\alpha)^{1/3}$
Power law	P4	$4(\alpha)^{3/7}$	$(\alpha)^{1/4}$	$4(\alpha)^{3/7}\times(\alpha)^{1/4}$
Avrami-Erofeyev	A2	$2(1-\alpha)[-ln(1-\alpha)]^{1/2}$	$[-ln(1-\alpha)]^{1/2}$	$2(1-\alpha)[-ln(1-\alpha)]^{1/2}\times[-ln(1-\alpha)]^{1/2}$
Avrami-Erofeyev	A3	$3(1-\alpha)[-ln(1-\alpha)]^{2/3}$	$[-ln(1-\alpha)]^{1/3}$	$3(1-\alpha)[-ln(1-\alpha)]^{2/3}\times[-ln(1-\alpha)]^{1/3}$
Avrami-Erofeyev	A4	$4(1-\alpha)[-ln(1-\alpha)]^{3/4}$	$[-ln(1-\alpha)]^{1/4}$	$4(1-\alpha)[-ln(1-\alpha)]^{3/4}\times[-ln(1-\alpha)]^{1/4}$
Geometrical contraction models				
Contracting area	R2	$2(1-\alpha)^{1/2}$	$1-(1-\alpha)^{1/2}$	$2(1-\alpha)^{1/2}\times1-(1-\alpha)^{1/2}$
Contracting vol.	R3	$3(1-\alpha)^{2/3}$	$1-(1-\alpha)^{1/3}$	$3(1-\alpha)^{2/3}\times1-(1-\alpha)^{1/3}$
Diffusion models				
1-dimensional	D1	$\frac{1}{2}(\alpha)$	$(\alpha)^2$	$\frac{1}{2}(\alpha)\times(\alpha)^2$
2-dimensional	D2	$-ln(1-\alpha)^{-1}$	$(1-\alpha)ln(1-\alpha)+\alpha$	$-ln(1-\alpha)^{-1}\times(1-\alpha)ln(1-\alpha)+\alpha$
3-dimensional	D3	$\frac{3(1-\alpha)^{2/3}}{2(1-(1-\alpha)^{1/3})}$	$\left[1-(1-\alpha)^{1/3}\right]^2$	$\frac{3(1-\alpha)^{1/2}}{2(1-(1-\alpha))^{1/3}}\times\left[1-(1-\alpha)^{1/3}\right]^2$
Reaction order models				
Zero order	F0	1	α	$1\times\alpha$
First order	F1	$(1-\alpha)$	$-ln(1-\alpha)$	$(1-\alpha)\times-ln(1-\alpha)$
Second order	F2	$(1-\alpha)^2$	$[1-(1-\alpha)^{-1}]/-1$	$(1-\alpha)^2\times[1-(1-\alpha)^{-1}]/-1$
Third order	F3	$(1-\alpha)^3$	$[1-(1-\alpha)^{-2}]/-2$	$(1-\alpha)^3\times[1-(1-\alpha)^{-2}]/-2$
Fourth order	F4	$(1-\alpha)^4$	$[1-(1-\alpha)^{-3}]/-3$	$(1-\alpha)^4\times[1-(1-\alpha)^{-3}]/-3$
Fifth order	F5	$(1-\alpha)^5$	$[1-(1-\alpha)^{-4}]/-4$	$(1-\alpha)^5\times[1-(1-\alpha)^{-4}]/-4$

$$ln\left(\frac{d\alpha}{dt}\right)=ln\left[\beta\left(\frac{d\alpha}{dT}\right)\right]=ln[k_o f(\alpha)^n]-\frac{E_\alpha}{RT_\alpha} \quad (8)$$

The E_α and k_o factors were calculated using the slope and intercept obtained from graphing $ln\left[\beta\left(\frac{d\alpha}{dT}\right)\right]$ vs. $\frac{1}{T_\alpha}$.

Kissinger-Akahira-Sunuse approach

Kissinger-Akahira-Sunuse (KAS) was proposed by Akahira and Sunuse (1971). Akahira and Sunnose (1971) employed the approximation $p(x)=x^{-2}exp^{-x}$ in Eq. (7); and the resultant mathematical equation, as follows:

$$ln\left(\frac{\beta}{T_\alpha^2}\right)=ln\left[\frac{k_o R}{E_\alpha g(\alpha)}\right]-\frac{E_\alpha}{RT_\alpha} \quad (9)$$

The E_α and k_o factors were obtained using the slope and intercept by graphing $ln\left(\frac{\beta}{T_\alpha^2}\right)$ vs. $\frac{1}{T_\alpha}$.

Ozawa-Flynn-Wall approach

Ozawa-Flynn-Wall (OFW) (Flynn & Wall, 1966), and Ozawa (1965) used Doyle's (1965) approximation $p(x)=\exp(-1.0516x-5.331)$ in Eq. (7); and the final expression was, as follows:

$$n\,(\beta)=ln\left[\frac{k_o E_\alpha}{Rg(\alpha)}\right]-5.331-1.0516\frac{E_\alpha}{RT_\alpha} \quad (10)$$

The E_α and k_o factors were calculated using the slope and intercept gained from graphing $ln(\beta)$ vs. $\frac{1}{T_\alpha}$.

Starink approach

Starink (STK) (Starink, 2003) used their own approximation $p(x)=\exp(-1.0008x-0.312)x^{1.92}$ in Eq. (7); and the resultant expression was, as follows:

$$n\left(\frac{\beta}{T_\alpha^{1.92}}\right)=ln\left[\frac{k_o R^{0.92}}{E_\alpha^{0.92}g(\alpha)}\right]-0.312-1.0008\frac{E_\alpha}{RT_\alpha} \quad (11)$$

The E_α and k_o factors were calculated using the slope and intercept gained from plotting $ln\left(\frac{\beta}{T_\alpha^{1.92}}\right)$ vs. $\frac{1}{T_\alpha}$.

Distributed activation energy approach

Distributed activation energy (DAE) was proposed by Miura and Maki (1998) used their own approximation $p(x)=0.6075-x$ in Eq. (7); and the outcome expression was, as follows:

$$nn\left(\frac{\beta}{T_\alpha^2}\right)=ln\left[\frac{k_o R}{E_\alpha}\right]+0.6075-\left[\frac{E_\alpha}{RT_\alpha}\right] \quad (12)$$

The E_α and k_o factors were calculated using the slope and intercept ascertained from plotting $ln\left(\frac{\beta}{T_\alpha^2}\right)$ vs. $\frac{1}{T_\alpha}$.

Predication of Reaction Mechanism

Criado's master plot approach

Reaction mechanism (Z_α) of pyrolysis of BRT waste was predicted by Criado's (Cradio et al., 1989) approach. The multiple reaction models were presented in **Table 1**, which includes differential (*f[α]*), integral (*g[α]*), and theoretical expressions.

$$Z(\alpha)_{Theo}=f(\alpha)_{Theo}\times g(\alpha)_{Theo} \quad (13)$$

$$Z(\alpha)_{Exp}=\left(\frac{d\alpha}{dt}\right)\times exp\left(\frac{E_\alpha}{RT}\right)\times\int_{T_0}^{T}exp\left(-\frac{E_\alpha}{RT}\right)dT \quad (14)$$

$$Z(\alpha)_{Exp}=\left(\frac{d\alpha}{dt}\right)\times\frac{E_\alpha}{R}\times exp\left(\frac{E_\alpha}{RT}\right)\times p(x) \quad (15)$$

$$Z(0.5)_{Exp}=\left(\frac{d\alpha}{dt}\right)\times\frac{E_{0.5}}{R}\times exp\left(\frac{E_{0.5}}{RT}\right)\times p(x) \quad (16)$$

where, $p(x)=0.00484\,exp\,(-1.0516x)$ (Doyle, 1965), Eq. (13), Eq. (14), Eq. (15), and Eq. (16) were used for the CMP studies (Alam et al., 2021a, 2021b; Irmak Aslan et al., 2017; Rammohan et al., 2022a, 2022b).

Thermodynamic Properties Estimation

Thermodynamic properties of pyrolysis of BRT waste were investigated in the study as presented below. The following Eq. (17), Eq. (18), and Eq. (19) were used for the thermodynamic studies (Balogun et al., 2021; Rammohan et al., 2022b; Singh et al., 2021; Volli et al., 2021; Wang et al., 2021):

Table 2. Physico-chemical characterization of butyl rubber tube waste

Sample	Proximate analysis (mass% on dry basis)			Ultimate analysis (mass % on dry basis-ash free)					H/C	O/C	HHV (MJ/kg)
	VM	FC	Ash	C	H	N	S	O			
BRT waste	56.66	33.76	10.26	57.99	6.22	-	1.1	35.73	1.28	0.82	22.06

Note. VM: Volatile matter; FC: Fixed carbon; C: Carbon; H: Hydrogen; N: Nitrogen; S: Sulfur; O: Oxygen; & HHV: Higher heating value

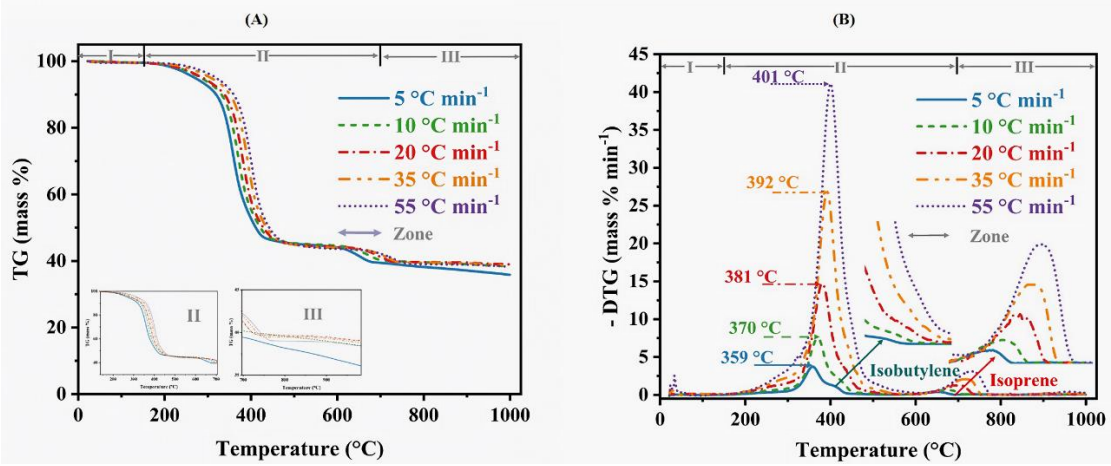

Figure 1. Thermal degradation of butyl rubber tube waste (A: TG and B: DTG) (Source: Authors' own elaboration)

$$k_o = \frac{\beta \times E_\alpha \times e^{\left(\frac{E_\alpha}{RT_m}\right)}}{RT_m^2} \quad (17)$$

Change in Gibbs free energy is, as follows:

$$\Delta G = E_\alpha + RT_m \times ln\left(\frac{K_B T_m}{hk_o}\right) \quad (18)$$

Change in enthalpy is, as follows:

$$\Delta H = E_\alpha - RT_m \quad (19)$$

where T_m represents temperature of peak decomposition (K), h represents Planck's constant (6.626×10^{-34} Js), and K_B represents Boltzmann constant (1.381×10^{-23} J K^{-1}).

Pyrolysis Performance Characteristics

BRT waste pyrolysis performance characteristics (PPC) such as devolatilization index, D_v (K^{-3} min^{-1}), combustion index, S (K^{-3} min^{-2}), burnout index, D_b (min^{-4}), ignition index, D_i (min^{-3}), and flammability index, C (K^{-2} min^{-1}) were reported using below equations (Balogun et al., 2021; Rammohan et al., 2022b; Wang et al., 2021; Wen et al., 2019):

$$C = \left(\frac{-R_p}{T_i^2}\right) \quad (20)$$

$$D_i = \left(\frac{-R_p}{t_i \times t_p}\right) \quad (21)$$

$$D_b = \left(\frac{-R_p}{\Delta t_{0.5} \times t_b \times t_p}\right) \quad (22)$$

$$S = \left(\frac{-R_p \times -R_v}{T_i^2 \times T_b}\right) \quad (23)$$

$$D_v = \left(\frac{-R_p \times -R_v}{\Delta T_{0.5} \times T_i \times T_p}\right) \quad (24)$$

where, R_p represents maximum rate of decomposition (mass% min^{-1}), R_v represents mean rate of decomposition (mass% min^{-1}), t_i represents time of ignition (min), t_b represents time of burnout (min), t_p represents maximum time of decomposition (min), $\Delta t_{0.5}$ represents half time of the R_p (min), T_i represents temperature of ignition (K), T_b represents temperature of burnout (K), T_p represents maximum temperature of decomposition (K), and $\Delta T_{0.5}$ represents half temperature of the R_p (K).

RESULTS AND DISCUSSIONS

Physicochemical Characterization

The physicochemical properties of BRT waste, including proximate analysis, ultimate analysis, and HHV values were shown in **Table 2**. Proximate analysis revealed that BRT waste with no moisture content was more susceptible to pyrolysis (Danon et al., 2015; Singh et al., 2021; Volli et al., 2021). BRT waste consists of volatile constituents (56.66%), and ash (10.26%) signifies its suitability for pyrolysis (Pradhan & Singh, 2015). The elemental analysis showed a carbon (57.99%), hydrogen (6.22%), and sulfur (1.1%), respectively, and no nitrogen components. This analysis was consistent with earlier results (Danon et al., 2015; Pradhan & Singh, 2015). Due to a linear relationship between carbon content and HHV, higher carbon content implies a better HHV (Khiari et al., 2018). HHV of the BRT waste (22.06 MJ kg^{-1}) concurs with NR, BR, SR, and SBR, and it is identified as a possible co-feedstock for the pyrolysis process (Aboelkheir et al., 2019; Khiariet al., 2018; Kordoghli et al., 2017a, 2017b; Lah et al., 2018; Pradhan & Singh, 2015).

Behavior of Thermal Degradation

During the pyrolysis process, the thermal degradation behavior of BRT waste was explored employing a non-isothermal mode thermogravimetric analyzer (TGA). TGA was operated at temperatures ranging from 25 to 1,000 °C in an inert environment (nitrogen) of 40 mL/min at varying heating rates (5, 10, 20, 35, and 55 °C min^{-1}). According to the TG pyrograms (**Figure 1**), the degradation of BRT waste could be classified into three zones (I, II, and III).

Table 3. Different zones of pyrolysis of thermal degradation of butyl rubber tube waste

Heating rate (°C min^{-1})	Zones											
	I (dehydration zone)				II (pyrolytic zone)				III (passive zone)			
	TG		DTG		TG		DTG		TG		DTG	
	T_{range} (°C)	Mass loss (mass%)	DT_{max} (°C)	DR_{max} (mass% min^{-1})	T_{range} (°C)	Mass loss (mass%)	DT_{max} (°C)	DR_{max} (mass% min^{-1})	T_{range} (°C)	Mass loss (mass%)	DT_{max} (°C)	DR_{max} (mass% min^{-1})
5	25-150	0.4	-	-	150-698	60	359	4	698-984	3.5	-	-
10	25-165	0.5	-	-	165-716	59.4	370	7	716-982	1.5	-	-
20	25-153	0.5	68	0.1	153-739	59.7	381	15	739-983	0.7	908	0.1
35	25-179	0.4	31	0.5	179-751	59.9	392	27	751-982	0.7	933	0.3
55	25-181	0.9	34	2.5	181-768	60.5	401	41	768-983	1	961	0.4

Note. DT_{max}: Maximum degradation temperature & DR_{max}: Maximum degradation rate

The devolatilization of BRT waste was described by two significant zones of mass loss during pyrolysis, as follows:

1. *Polymeric components→Volatile 1 + Radical 1* (*main split of the chain*)
2. *Depolmerization reactions*:
   a. *Radical 1→Volatile 2*
   b. *Radical 1→Radical 2*
   c. *Radical 2→Volatile 3*
3. *Radical 2→Radical 3* (*cyclization reactions*)
4. *Radical 3→Volatile 4 + Radical 4* (*cyclic products degradation*).

For the above reaction steps, initially, the polymeric components (isobutylene and isoprene) present in BRT were fragmented into volatile 1 compounds (monomers) and stable radical 1 (H_2, CH_4, and CO) at lower temperatures according to Aboelkheir et al. (2019), Kordoghil et al. (2017a, 2017b), and Qu et al. (2020). Then, the radicals were further transformed into volatile compounds (dimers/trimers) by depolymerization reaction at intermediate temperatures. Following that, intermediate radical products were further cracked to yield stable radical 3 products such as aliphatic, aromatic, and H_2S via cyclization reactions (Danon et al., 2015; Kardoghli et al., 2017a, 2017b; Khiari et al., 2018; Nkosi et al., 2021). Finally, the stable radical 3 products were further degraded to volatile 4 and radical 4 products such as alkenes, alkanes, and solid char at higher temperatures (Khiari et al., 2018). A free radical reaction mechanism contributes significantly to the decomposition of BRT waste. The chain scission primarily occurred at the β-position of the BRT (Aboelkheir et al., 2019; Xu et al., 2018). Through the scission and dehydrogenation reactions, the 2-butenyl radical obtained from scission was converted to 1,3-butadiene.

Furthermore, chain scission can give rise to other free radicals, which can then rearrange into C_5- and C_7-radical species. The C_5- and C_7-radical species can be cyclized to form 1,3- and 1,4-cyclooctadiene. Due to the fact that the C-C single bond in -C-C=C- was much stronger than the one in -C-C-C-, the rearrangement of -C-C=C- in C_5 and C_7 radical species can occur only at higher temperatures (T>800 °C) during the pyrolysis of BRT (Aboelkheir et al., 2019; Xu et al., 2018). The pyrolysis pathways of major pyrolytic components such as isoprene, isobutylene, 1,3-butadiene, 1,3-and 1,4-cyclopentadiene had a significant effect on the pyrolysis of BRT (Aboelkheir et al., 2019; Xu et al., 2018).

From the TG and DTG results (A & B in **Figure 1** and **Table 3**), it was observed that the minor fractions such as plasticizers, oils, and additives were removed at the temperature range from 25-180 °C in the zone I (Khiari et al., 2018; Peñalver et al., 2021; Pradhan & Singh, 2015). At this zone, negligible mass losses from 0.4 to 0.9 mass% were observed at all heating rates of 5-55 °C min^{-1}. The major devolatilization of BRT waste was elucidated at the temperature range from 180 °C to 768 °C in zone II. It was noticed that in this zone II, the formation of radicals and high conversion of BRT took place rapidly. Several reactions, such as depolymerization and cyclization, occurred with maximum mass loss. The maximum mass losses were from 59.4 to 60.5 mass% and were ascertained for increased heating rates in the order of 5-50 °C min^{-1}. The pyrograms revealed that higher heating rates resulted in increased decomposition of BRT material. The maximum decomposition of BRT occurred at 359, 370, 381, 392, and 401 °C. The temperature shift was due to increased heating rate delay (Dziemidkiewicz et al., 2019; Han et al., 2018; Neves et al., 2022; Qui et al., 2022). Moreover, at a higher heating rate of 50 °C min^{-1}, the maximum DTG (rate of mass loss) was increased (Dziemidkiewicz et al., 2019; Han et al., 2018; Qui et al., 2022). Three peaks of DTG pyrograms for every heating rate signify the major devolatilization of BRT, isobutylene, and isoprene, respectively. Similar kinds of pyrograms trends were reported elsewhere (Peñalver et al., 2021; Pradhan & Singh, 2015; Rammohan et al., 2022b). Furthermore, from B in **Figure 1**, the peaks at 390-459 °C and 620-783 °C indicated that isobutylene and isoprene disintegrated between the temperatures of 390-435 °C and 620-687 °C at 5 °C min^{-1}; 402-450 °C and 632-709 °C at 10 °C min^{-1}; 421-456 °C and 635-737 °C at 20 °C min^{-1}; 435-458 °C and 641-754 °C at 35 °C min^{-1}; 447-459 °C and 636-783 °C at 55 °C min^{-1} correspondingly (Kawale & Kishore, 2021; Pradhan & Singh, 2015). Additionally, no sharp peaks were observed for the undecomposed solid char at temperatures above 800 °C (Han et al., 2018; Xu et al., 2018; Volli et al., 2021). Finally, because of more secondary reactions (cyclization products degradation) between IIR co-polymers, approximately 45-55 mass% (for 5-55 °C min^{-1} of heating rates) of the tube waste remains undecomposed and may lead to solid char by the end of pyrolysis (Han et al., 2018; Kawale & Kishore, 2021; Nkosi et al., 2021; Pradhan & Singh, 2015).

Estimation of Kinetics

Kinetic triplets (KT) including activation energy (E_α), pre-exponential factor (k_o), and model of the reaction mechanism (Z_α) were evaluated for the pyrolytic decomposition of BRT waste by using five iso-conversional approaches. Five iso-conversional approaches (DFM, OFW, KAS, DAE, and STK) and five heating rates (β) (5, 10, 20, 35, and 55 °C min^{-1}) were

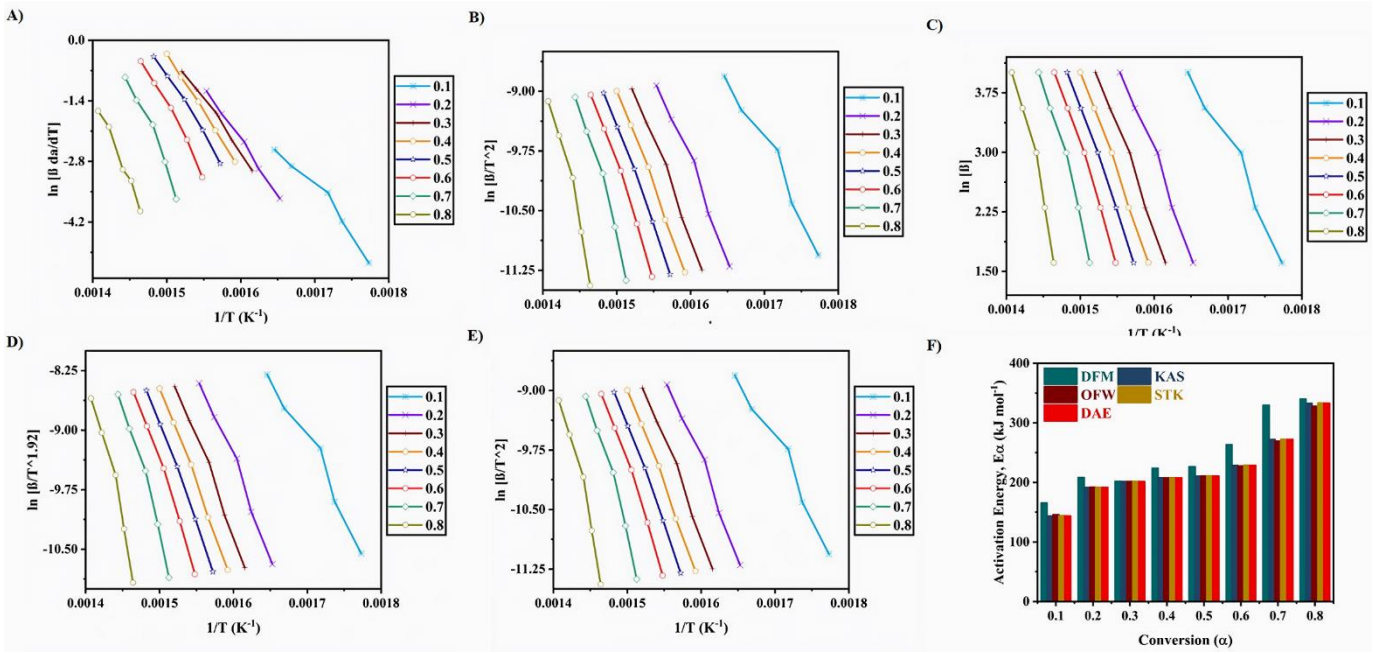

Figure 2. Iso-conversional plots by A: DFM, B: KAS, C: OFW, D: STK, E: DAE, and F: Activation energy vs. conversion plot for all five approaches (Source: Authors' own elaboration)

Table 4. Activation energy & pre-exponential factor from various iso-conversional approaches for BRT waste pyrolysis

α	DFM			KAS			OFW			STK			DAE		
	E_α	k_o	R^2	E_α	k_o	R^2	E_α	k_o	R^2	E_α	k_o	R^2	E_α	k_o	R^2
0.1	165.12	1.56E+13	0.96	143.47	6.16E+11	0.97	145.70	5.17E+09	0.97	143.75	5.1E+11	0.97	143.47	5.79E+12	0.97
0.2	208.12	3.06E+16	0.99	191.49	2.58E+15	0.98	191.96	1.40E+13	0.99	191.75	2.1E+15	0.98	191.49	1.13E+16	0.98
0.3	201.54	7.56E+15	0.99	201.10	1.12E+16	0.99	201.33	5.73E+13	0.99	201.37	9.0E+15	0.99	201.10	3.05E+16	0.99
0.4	223.90	4.32E+17	0.99	207.31	2.94E+16	0.99	207.37	1.46E+14	0.99	207.58	2.4E+16	0.99	207.31	5.64E+16	0.99
0.5	226.26	4.83E+17	0.99	210.32	4.29E+16	0.99	210.36	2.13E+14	0.99	210.59	3.5E+16	0.99	210.32	6.14E+16	0.99
0.6	263.59	2.51E+20	0.98	228.25	9.41E+17	0.99	227.55	4.08E+15	0.99	228.51	7.6E+17	0.99	228.25	1.01E+18	0.99
0.7	329.59	1.16E+25	0.97	272.10	1.66E+21	0.98	269.44	5.28E+18	0.98	272.33	1.3E+21	0.98	272.10	1.36E+21	0.98
0.8	339.72	1.02E+25	0.98	332.94	2.40E+25	0.96	327.62	5.45E+22	0.97	333.13	1.9E+25	0.96	332.94	1.48E+25	0.96
Mean	244.73	2.73E+24	0.987	223.37	3.00E+24	0.987	222.67	6.82E+21	0.988	223.63	2.35E+24	0.987	223.37	1.84E+24	0.987

Note. α: Conversion; E_α: Activation energy (kJ mol^{-1}); & k_o: Pre-exponential factor (min^{-1})

employed for the investigation of E_α, and k_o. DFM graph was generated from Eq. (8) by drawing $ln\left[\beta\left(\frac{d\alpha}{dT}\right)\right]$ vs. 1/T, as provided in A in **Figure 2**.

In addition, (E_α) and (k_o) were calculated by associating the slope $\left(\frac{-E_\alpha}{R}\right)$ and intercept throughout the conversion (0.1 to 0.8) limit and these results were presented in **Table 4**.

Similarly, plots and data for the other approaches KAS, OFW, STK, and DAE (according to Eq. [9], Eq. [10], Eq. [11], and Eq. [12], respectively), were presented in B-E in **Figure 2**, respectively and **Table 4**. The experimental kinetic results were fitted well (R^2>0.98) between 0.1 to 0.8 conversion. Secondary reactions (cyclization product degradation) that produced significant amounts of solid residues (char/ash) occurred at conversions greater than 0.8 during BRT pyrolysis (Han et al., 2018; Xu et al., 2018). From the findings (F in **Figure 2** and **Table 4**), E_α (kJ mol^{-1}), and k_o (min^{-1}) were 244.73 and 2.73×10^{24}; 223.37 and 3×10^{24}; 222.67 and 6.52×10^{21}; 223.63 and 2.35×10^{24}; 223.37 and 1.84×10^{24}; obtained respectively for all five approaches. It was observed that from 0.1 to 0.8 conversion, the OFW and KAS approaches yielded the lowest kinetic parameters 222.67 and 223.37 (kJ mol^{-1}) respectively. The values of E_α were presented for pyrolysis of MPW by Singh et al. (2019) using KAS and OFW approaches were 175 and 178 kJ mol^{-1}, respectively; for PE by Singh et al. (2021) using DFM and OFW approaches were 171 and 159 kJ mol^{-1}, respectively; and for NR, SR, BR, and SBR by Danon et al. (2015) using DFM approach were 434, 372, 409, and 305 kJ mol^{-1}, respectively.

Table 5 depicted a comparison of the present mean kinetics findings with published literature counterparts. According to the findings of kinetic studies, the mean E_α values of BRT pyrolysis was lower and more significant than SBR. Thus, pyrolysis of the BRT waste may be more energy-efficient than SBR based on the activation energies found. However, a comparable trend of E_α was evidenced between the conversions of 0.1 to 0.8 for all iso-conversional approaches (Danon et al., 2015; Han et al., 2018; Xu et al., 2018) [22,46,48].

From the kinetic results (F in **Figure 2** and **Table 4**), the alterations in E_α and k_o (10^{15} to 10^{16}) were increased between conversion of 0.1 to 0.3 as a result of a reaction on the surface of BRT waste, which indicates degradation of isobutylene polymer (to volatile 1 compounds (monomers) and radical 1 by depolymerization) as per Kordoghli et al. (2017a, 2017b) and then E_α and k_o (order of <10^{15}) decreases marginally up to conversion of 0.6, in which the isoprene polymer was degraded (to radicals and volatile compounds (dimers/trimers) by

Table 5. Comparison of kinetic & thermodynamic parameters of pyrolysis of different synthetic polymers & BRT of present study

Feed	DFM			KAS			OFW			STK			DAE			Ref.
	E_α (kJ mol^{-1})	ΔH (kJ mol^{-1})	ΔG (kJ mol^{-1})	E_α (kJ mol^{-1})	ΔH (kJ mol^{-1})	ΔG (kJ mol^{-1})	E_α (kJ mol^{-1})	ΔH (kJ mol^{-1})	ΔG (kJ mol^{-1})	E_α (kJ mol^{-1})	ΔH (kJ mol^{-1})	ΔG (kJ mol^{-1})	E_α (kJ mol^{-1})	ΔH (kJ mol^{-1})	ΔG (kJ mol^{-1})	
BRT waste	244.73	239.38	185.44	223.37	218.03	214.46	222.67	217.32	185.93	223.63	218.28	185.92	223.37	218.03	185.93	PS
MP waste	-	-	-	175.36	-	-	177.94	172.14	159.76	-	-	-	-	-	-	20
PE	171	176	222	156	-	-	159	-	-	148	-	-	-	-	-	21
NR, SR, BR, SBR	434 for NR, 372 for SR, 409 for BR, 305 for SBR	-	-	-	-	-	-	-	-	-	-	-	-	-	-	22

Note. BRT: Butyl rubber tube; MP: Milk packet; PE: Poly ethylene; NR: Natural rubber; SR: Synthetic rubber; BR: Butadiene rubber; SBR: Styrene-butadiene-rubber; PS: Present study; 20: Singh et al. (2019); 21: Singh et al. (2021); & 22: Danon et al. (2015)

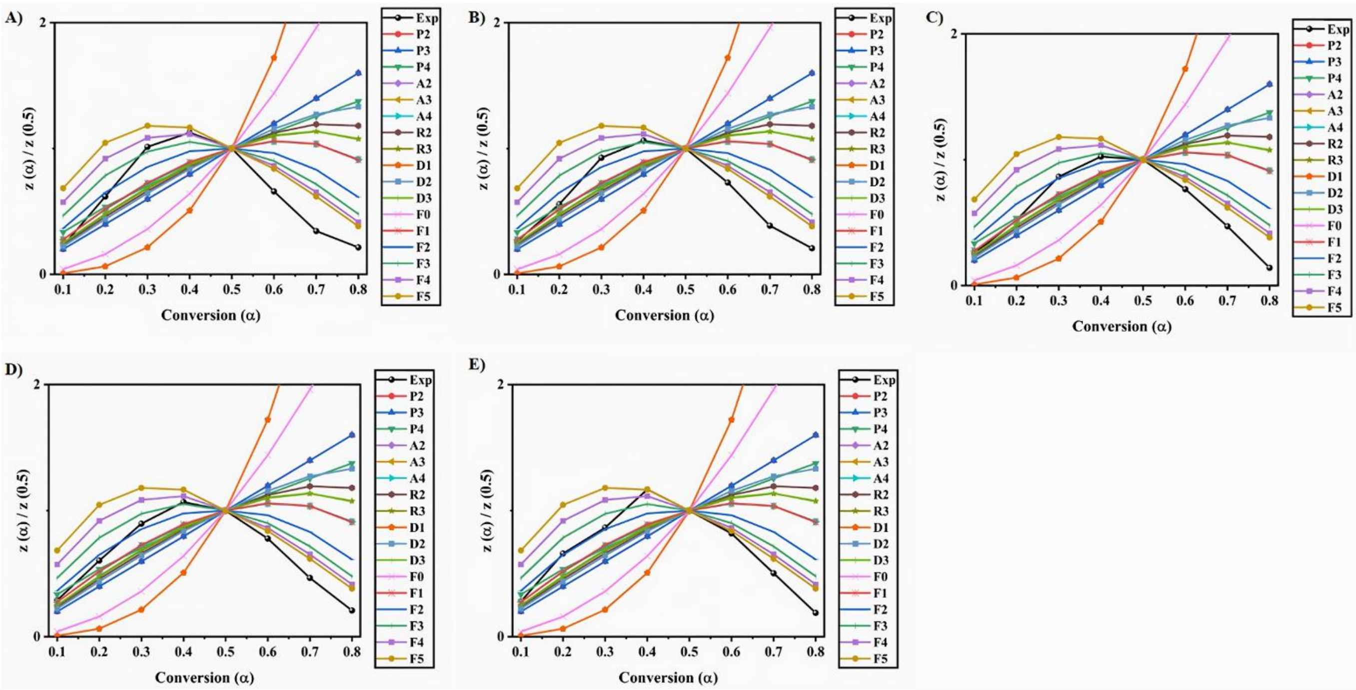

Figure 3. Possible mechanism of pyrolysis of BRT waste by Criado's master method at multiple heating rates (A: 5°C min^{-1}, B: 10°C min^{-1}, C: 20°C min^{-1}, D: 35°C min^{-1}, & E: 55°C min^{-1}) (Source: Authors' own elaboration)

Table 6. Possible mechanism of pyrolysis of butyl rubber tube waste by Criado's master method at multiple heating rates

Conversion (α)	Heating rate (°C min^{-1})				
	5	10	5	35	5
0.1	D2	A4	D3	F1	F1
0.2	F2	P4	F1	F2	F2
0.3	D3	F3	F2	F2	F2
0.4	F4	F3	F3	F3	F5
0.5	-	-	-	-	-
0.6	>F5	>F5	>F5	>F5	F5
0.7	>F5	>F5	>F5	>F5	>F5
0.8	>F5	>F5	>F5	>F5	>F5

Note. Reaction mechanism models: P2 & P3: Second & third power law models; A4: Fourth Avrami-Erofeyev model; R2 & R3: Area & volume contracting models; D2 & D3: 2- & 3-dimensional diffusion models; & F1, F2, F3, & F5: First, second, third, & five reaction order models

cyclization reaction), and then E_α and k_o (order of >10^{17}) increases progressively up to conversion of 0.8 as a result of frequent collisions between molecules (to form volatile 4 and radical 4 by cyclic degradation), thus pyrolysis of BRT waste requires a significant amount of energy (Khiari et al., 2018; Kordoghli et al., 2017a, 2017b; Nkosi et al., 2021).

According to E_α and k_o findings, as the rate of heating increases, the rate of collisions between the molecules increases, causing the faster rate of reaction for BRT waste pyrolysis. Due to the heterogeneity of BRT waste, the major polymeric components such as isobutylene and isoprene were decomposed at different temperatures as demonstrated by changes in E_α and k_o as per studies of Danon et al. (2015) and Nkosi et al. (2021). Therefore, the pyrolysis of BRT waste goes through a complex reaction with a multi-step mechanism.

From the Criado's plot analysis, the reaction mechanism was predicted for the pyrolysis of BRT waste. Criado's graphs were derived from Eq. (13), Eq. (14), Eq. (15), and Eq. (16) by plotting a plot of z(α)/z(0.5) vs. α, and provided in A-E in **Figure 3** and **Table 6** for each for each heating rate.

For example, at 20 °C min^{-1}, it was observed that the experimental result indicated a trend of 3-dimensional diffusion (D3) and first-order (F1) at α=0.1 to 0.2, second (F2) and third-order (F3) at α = 0.3 to 0.4, and then higher-order reaction (>F5) at α=0.6 to 0.8. Finally, the master plot analysis demonstrated that the pyrolysis of BRT waste exhibited a multistep reaction mechanism.

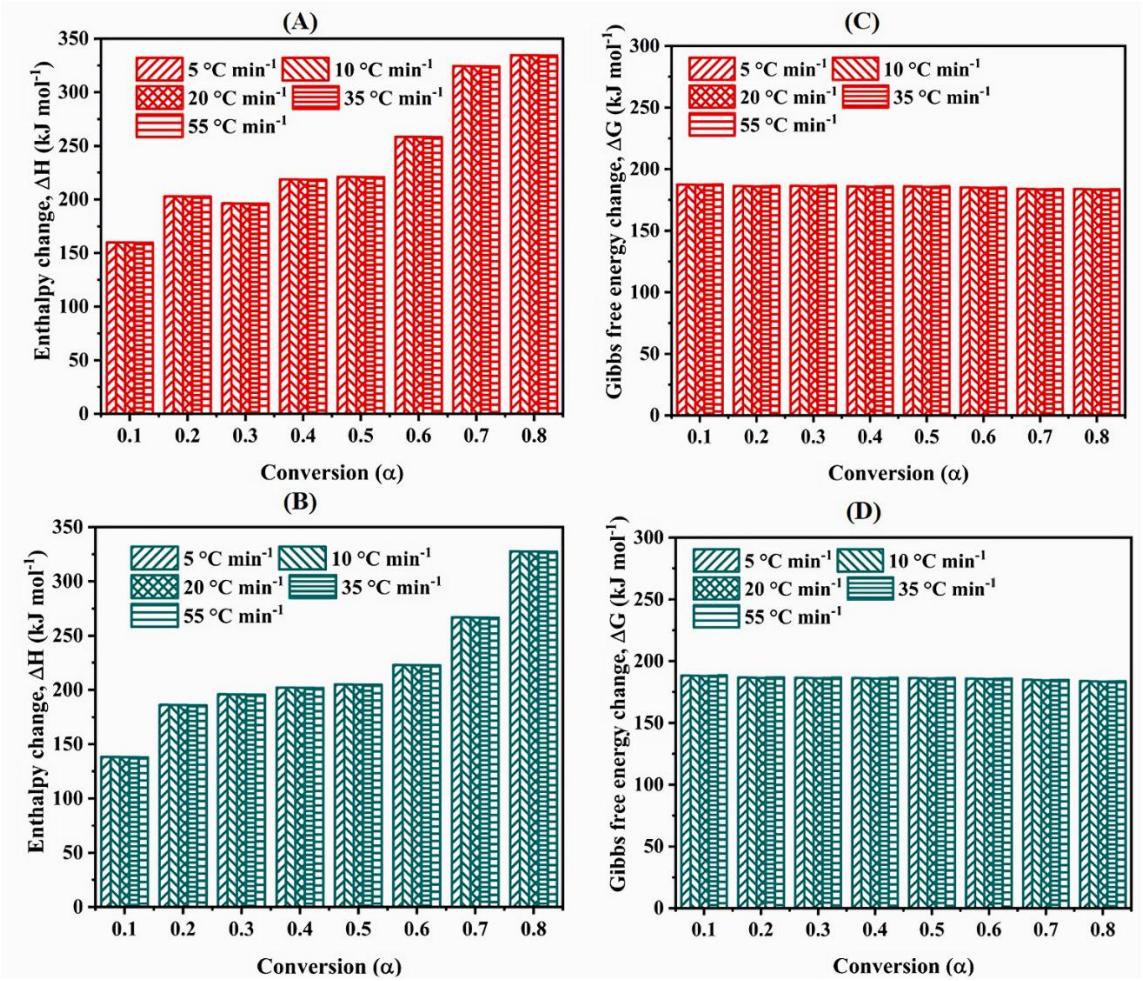

Figure 4. Thermodynamic parameters of pyrolysis of BRT waste (A & B: Change in enthalpy, C & D: Change in Gibbs free energy from DFM & DAE approaches) (Source: Authors' own elaboration)

Estimation of Thermodynamics

Thermodynamic parameters of pyrolysis of BRT waste, such as enthalpy change (ΔH), Gibbs free energy change (ΔG), and pre-exponential factor (k_o), were evaluated and depicted in **Figure 4** and **Table 7**.

Thermodynamic assessments were calculated employing Eq. (17), Eq. (18), and Eq. (19) for DFM, KAS, OFW, STK, and DAE approaches. The results included thermodynamic parameters of pyrolysis of BRT waste via DFM and DAE (**Figure 4**), while **Table 7** included those by KAS, OFW, and STK approaches. A-B in **Figure 4** depicts ΔH vs. α variations for both DFM and DAE approaches. A-B in **Figure 4** illustrated that the effect of heating rate on ΔH seems to be negligible. Variations in E_α dependent upon α, also influenced the variation in enthalpy.

Table 7. Thermodynamic properties of butyl rubber tube waste at multiple heating rate (β)

α	DFM			KAS			OFW			STK			DAE		
	k_o	ΔH	ΔG	k_o	ΔH	ΔG	k_o	ΔH	ΔG	k_o	ΔH	ΔG	k_o	ΔH	ΔG
(β=5 °C min^{-1})															
0.1	1.84E+11	159.86	187.56	2.60E+09	138.22	188.30	4.03E+09	140.44	188.22	2.74E+09	138.49	188.29	2.60E+09	138.22	188.30
0.2	8.32E+14	202.87	186.34	3.23E+13	186.23	186.78	3.54E+13	186.71	186.77	3.40E+13	186.50	186.77	3.23E+13	186.23	186.78
0.3	2.30E+14	196.29	186.51	2.11E+14	195.85	186.52	2.21E+14	196.07	186.52	2.22E+14	196.11	186.52	2.11E+14	195.85	186.52
0.4	1.80E+16	218.64	185.96	7.10E+14	202.06	186.36	7.18E+14	202.11	186.36	7.47E+14	202.32	186.36	7.10E+14	202.06	186.36
0.5	2.85E+16	221.00	185.90	1.28E+15	205.07	186.29	1.29E+15	205.10	186.29	1.35E+15	205.33	186.28	1.28E+15	205.07	186.29
0.6	4.04E+19	258.33	185.10	5.73E-03	223.00	414.11	3.67E+16	222.30	185.87	4.42E+16	223.25	185.85	4.20E+16	223.00	185.86
0.7	1.44E+25	324.33	183.93	2.11E+20	266.84	184.93	1.26E+20	264.19	184.99	2.20E+20	267.07	184.93	2.11E+20	266.84	184.93
0.8	1.02E+26	334.47	183.77	2.76E+25	327.68	183.87	9.85E+24	322.36	183.96	2.86E+25	327.88	183.87	2.76E+25	327.68	183.87
Mean	1.46E+25	239.48	185.63	3.44E+24	218.12	214.65	1.23E+24	217.41	186.12	3.58E+24	218.37	186.11	3.44E+24	218.12	186.12
(β=10 °C min^{-1})															
0.1	2.08E+11	159.77	187.40	3.15E+09	138.13	188.15	4.84E+09	140.35	188.06	3.32E+09	138.40	188.14	3.15E+09	138.13	188.15
0.2	8.16E+14	202.78	186.16	3.34E+13	186.14	186.60	3.66E+13	186.62	186.59	3.51E+13	186.40	186.60	3.34E+13	186.14	186.60
0.3	2.31E+14	196.19	186.33	2.12E+14	195.76	186.34	2.21E+14	195.98	186.34	2.23E+14	196.02	186.33	2.12E+14	195.76	186.34
0.4	1.68E+16	218.55	185.77	6.98E+14	201.97	186.18	7.06E+14	202.02	186.18	7.35E+14	202.23	186.17	6.98E+14	201.97	186.18
0.5	2.64E+16	220.91	185.71	1.24E+15	204.98	186.10	1.25E+15	205.01	186.10	1.31E+15	205.24	186.09	1.24E+15	204.98	186.10

Table 7 (Continued). Thermodynamic properties of butyl rubber tube waste at multiple heating rate (β)

α	DFM			KAS			OFW			STK			DAE		
	k_o	ΔH	ΔG	k_o	ΔH	ΔG	k_o	ΔH	ΔG	k_o	ΔH	ΔG	k_o	ΔH	ΔG
0.6	3.31E+19	258.24	184.89	1.11E-02	222.90	413.91	3.38E+16	222.20	185.68	4.06E+16	223.16	185.66	3.86E+16	222.90	185.66
0.7	9.53E+24	324.24	183.70	1.68E+20	266.75	184.72	1.01E+20	264.10	184.78	1.76E+20	266.98	184.72	1.68E+20	266.75	184.72
0.8	6.54E+25	334.38	183.54	1.80E+25	327.59	183.65	6.55E+24	322.27	183.73	1.87E+25	327.79	183.64	1.80E+25	327.59	183.65
Mean	9.36E+24	239.38	185.44	2.25E+24	218.03	214.46	8.19E+23	217.32	185.93	2.34E+24	218.28	185.92	2.25E+24	218.03	185.93
(β=20 °C min^{-1})															
0.1	2.39E+11	159.68	187.11	3.87E+09	138.04	187.87	5.92E+09	140.26	187.79	4.08E+09	138.31	187.86	3.87E+09	138.04	187.87
0.2	8.20E+14	202.69	185.85	3.54E+13	186.05	186.30	3.87E+13	186.52	186.29	3.72E+13	186.31	186.30	3.54E+13	186.05	186.30
0.3	2.36E+14	196.10	186.02	2.18E+14	195.67	186.04	2.27E+14	195.89	186.03	2.29E+14	195.93	186.03	2.18E+14	195.67	186.04
0.4	1.60E+16	218.46	185.45	7.03E+14	201.87	185.87	7.11E+14	201.93	185.87	7.39E+14	202.14	185.86	7.03E+14	201.87	185.87
0.5	2.50E+16	220.82	185.40	1.24E+15	204.88	185.79	1.25E+15	204.92	185.79	1.30E+15	205.15	185.79	1.24E+15	204.88	185.79
0.6	2.79E+19	258.15	184.57	2.14E-02	222.81	413.60	3.19E+16	222.11	185.36	3.82E+16	223.07	185.34	3.64E+16	222.81	185.35
0.7	6.53E+24	324.15	183.35	1.38E+20	266.66	184.39	8.39E+19	264.01	184.45	1.44E+20	266.89	184.39	1.38E+20	266.66	184.39
0.8	4.34E+25	334.29	183.19	1.22E+25	327.50	183.30	4.52E+24	322.18	183.38	1.27E+25	327.70	183.29	1.22E+25	327.50	183.30
Mean	6.24E+24	239.29	185.12	1.53E+24	217.94	214.15	5.65E+23	217.23	185.62	1.58E+24	218.19	185.61	1.53E+24	217.94	185.61
(β=35 °C min^{-1})															
0.1	2.45E+11	159.59	187.44	4.24E+09	137.94	188.22	6.43E+09	140.17	188.13	4.46E+09	138.22	188.20	4.24E+09	137.94	188.22
0.2	7.37E+14	202.60	186.16	3.34E+13	185.96	186.62	3.65E+13	186.43	186.61	3.51E+13	186.22	186.61	3.34E+13	185.96	186.62
0.3	2.17E+14	196.01	186.34	2.00E+14	195.58	186.35	2.08E+14	195.80	186.34	2.10E+14	195.84	186.34	2.00E+14	195.58	186.35
0.4	1.37E+16	218.37	185.75	6.33E+14	201.78	186.18	6.40E+14	201.84	186.18	6.65E+14	202.05	186.17	6.33E+14	201.78	186.18
0.5	2.13E+16	220.73	185.70	1.11E+15	204.79	186.10	1.11E+15	204.83	186.10	1.16E+15	205.06	186.09	1.11E+15	204.79	186.10
0.6	2.12E+19	258.06	184.85	3.62E-02	222.72	413.90	2.70E+16	222.02	185.67	3.23E+16	222.98	185.64	3.08E+16	222.72	185.65
0.7	4.05E+24	324.06	183.62	1.02E+20	266.57	184.68	6.25E+19	263.92	184.73	1.06E+20	266.80	184.67	1.02E+20	266.57	184.68
0.8	2.61E+25	334.19	183.45	7.51E+24	327.41	183.56	2.82E+24	322.09	183.65	7.78E+24	327.61	183.56	7.51E+24	327.41	183.56
Mean	3.77E+24	239.20	185.41	9.38E+23	217.84	214.45	3.53E+23	217.14	185.93	9.73E+23	218.10	185.91	9.38E+23	217.84	185.92
(β=55 °C min^{-1})															
0.1	2.51E+11	159.52	187.67	4.59E+09	137.87	188.46	6.92E+09	140.09	188.37	4.82E+09	138.14	188.45	4.59E+09	137.87	188.46
0.2	6.82E+14	202.52	186.37	3.22E+13	185.88	186.84	3.51E+13	186.36	186.82	3.38E+13	186.15	186.83	3.22E+13	185.88	186.84
0.3	2.04E+14	195.94	186.55	1.88E+14	195.50	186.56	1.96E+14	195.72	186.56	1.97E+14	195.76	186.56	1.88E+14	195.50	186.56
0.4	1.22E+16	218.30	185.96	5.87E+14	201.71	186.39	5.93E+14	201.77	186.39	6.16E+14	201.97	186.39	5.87E+14	201.71	186.39
0.5	1.88E+16	220.65	185.90	1.02E+15	204.72	186.31	1.03E+15	204.75	186.31	1.07E+15	204.99	186.31	1.02E+15	204.72	186.31
0.6	1.72E+19	257.98	185.05	5.54E-02	222.65	414.10	2.39E+16	221.95	185.87	2.84E+16	222.91	185.85	2.71E+16	222.65	185.85
0.7	2.80E+24	323.98	183.80	8.09E+19	266.49	184.87	4.99E+19	263.84	184.92	8.44E+19	266.72	184.86	8.09E+19	266.49	184.87
0.8	1.76E+25	334.12	183.63	5.14E+24	327.33	183.74	1.96E+24	322.01	183.83	5.33E+24	327.53	183.74	5.14E+24	327.33	183.74
Mean	2.55E+24	239.13	185.62	6.42E+23	217.77	214.66	2.45E+23	217.06	186.13	6.66E+23	218.02	186.12	6.42E+23	217.77	186.13

Note. α: Conversion; k_o: Pre-exponential factor; & ΔH & ΔG: Change in enthalpy & Gibbs free energy (kJ mol^{-1})

Table 8. Pyrolysis performance characteristics of pyrolysis of BRT waste at multiple heating rates

β	T_i	T_p	T_b	$\Delta T_{0.5}$	t_i	t_p	t_b	$\Delta t_{0.5}$	$-R_p$	$-R_v$	C	D_i	D_b	S	D_v
5	561	632	1248	608	4.8	4	190	62	3.7	0.3	1.18E-05	1.93E-01	7.85E-05	2.83E-09	5.15E-09
10	573	643	1216	618	27.5	7	91.9	32	7.5	0.6	2.28E-05	3.90E-02	3.64E-04	1.13E-08	1.98E-08
20	580	654	1185	628	14.1	15	39.3	16.5	14.7	1.2	4.37E-05	6.95E-02	1.51E-03	4.43E-08	7.41E-08
35	594	665	1202	640	8.4	27	39.1	9.8	26.8	2.1	7.60E-05	1.18E-01	2.59E-03	1.33E-07	2.23E-07
55	601	674	1212	646	5.5	41	16.6	6.3	41.1	3.4	1.14E-04	1.82E-01	9.59E-03	3.19E-07	5.34E-07

At α=0.8 conversion, the maximum values of ΔH were 183.77 kJ mol^{-1} for DFM and 183.87 kJ mol^{-1} for DAE approaches, correspondingly. From 0.1 to 0.8 conversion, a positive value of ΔH was observed, revealing that the pyrolysis of BRT waste was endothermic in nature. Additionally, as the enthalpy change was increased from 0.1 to 0.8 conversion, the endothermicity of pyrolysis of BRT waste increased. Furthermore, change in Gibbs free energy (ΔG) vs. (α) variations were illustrated in C-D in **Figure 4**.

Minor differences in ΔG were noticed (between α=0.1 to 0.8), with the major values being 185.63 kJ mol^{-1}, and 183.87 kJ mol^{-1} for the DFM and DAE approaches, correspondingly.

Furthermore, **Table 5** illustrated a comparison between mean thermodynamic parameters obtained in the present work and with existing literature reports.

Pyrolysis Performance Characteristics

PPC of the BRT waste were provided in **Table 8**. From the tabulated data, it was observed that all the characteristic values such as flammability (C), ignition (D_i), burnout (D_b), combustion (S), and devolatilization (D_v) of pyrolysis of BRT waste were increased with heating rates (5 to 55°C min^{-1}).

Also, as the heating rates, increased the values of temperatures (ignition T_i, degradation T_p, burnout T_b) and times (ignition t_i, degradation t_p, burnout t_b) factors of pyrolysis of BRT waste were increased and decreased, respectively. The higher C value of BRT waste was (1.14×10^{-4}) observed at 55°C min^{-1} because of lower moisture content. The higher D_i and D_b values of pyrolysis of BRT waste (1.82×10^{-1} and 9.59×10^{-3}) indicated the good combustion ability. The higher S value of pyrolysis of BRT waste (3.19×10^{-7}) suggested a better combustion performance.

The higher D_v value of pyrolysis of BRT waste (5.34×10^{-7}) reveals the formation of the more volatile matter when it was subjected to pyrolysis. The ascertained PPC findings of the current research work were consistent with the other reports (Rammohan et al., 2022b; Singh et al., 2021).

CONCLUSIONS

In this work, BRT was pyrolyzed in a TGA so that to examine its thermal degradation behavior, kinetics, reaction mechanism, thermodynamic properties and PPC. The following conclusions were drawn from the results of the present work:

- Pyrolysis of BRT waste occurred in the temperature between 150 and 768 °C resulting highest mass loss of about ≈60 wt.%.
- The activation energy (E_α) by DFM, KAS, OFW, STK, and DAE was estimated to be between 222.67 and 244.73 kJ mol^{-1}. Among all approaches, OFW model (222.67 kJ mol^{-1}) is the lowest energy demanding and propinquity to KAS model (223.37 kJ mol^{-1}).
- The pre-exponential factor (k_o) altered between 6.82×10^{21} and 2.73×10^{24} s^{-1}, demonstrated a higher reaction rate of BRT waste during pyrolysis.
- In accordance with Criado's master plots (CMP), multi reaction mechanism were observed for all the heating rates (5-55 °C min^{-1}) throughout the present range of conversion (0.1-0.8).
- Based on the thermodynamic findings, the mean values of ΔH and ΔG, respectively, were 183.77 kJ mol^{-1} and 183.87 kJ mol^{-1} from DAE, exhibited the endothermic and non-spontaneous reactions. Furthermore, a variation of 40 kJ mol^{-1} was found between the mean E_α and ΔH values from DAE, implying that a considerable amount of energy corresponding to ΔH must be supplied for pyrolysis to proceed.
- In addition, the higher PPC of BRT waste were recorded. These included (C=1.14×10^{-4}), ignition (D_i=1.82×10^{-1}), burnout (D_b=9.59×10^{-3}), combustion (S=3.19×10^{-7}) and devolatilization (D_v=5.34×10^{-7}).

Author contributions: All co-authors have involved in all stages of this study while preparing the final version. They all agree with the results and conclusions.

Funding: No funding source is reported for this study.

Declaration of interest: No conflict of interest is declared by the authors.

Ethical statement: The authors stated that they have reviewed the ethics committee requirement on publications and manuscript submission and complied with it in reviewing this manuscript.

Data sharing statement: Data supporting the findings and conclusions are available upon request from corresponding author.

REFERENCES

Aboelkheir, M. G., Visconte, L. Y., Oliveira, G. E., Toledo Filho, R. D., & Souza, F. G. (2019). The biodegradative effect of tenebrio molitor linnaeus larvae on vulcanized SBR and tire crumb. *Science of The Total Environment, 649*, 1075-1082. https://doi.org/10.1016/j.scitotenv.2018.08.228

Akahira, T., & Sunuse, T. T. (1971). Joint convection of four electrical institues. *Chiba Institute of Technology*. https://www.scirp.org/(S(i43dyn45teexjx455qlt3d2q))/reference/ReferencesPapers.aspx?ReferenceID=431880

Alam, M., Rammohan, D., & Peela, N. R. (2021b). Catalytic co-pyrolysis of wet-torrefied bamboo sawdust and plastic over the zeolite H-zsm-5: Synergistic effects and kinetics. *Renewable Energy, 178*, 608-619. https://doi.org/10.1016/j.renene.2021.06.109

Alam, M., Rammohan, D., Bhavanam, A., & Peela, N. R. (2021a). Wet torrefaction of bamboo saw dust and its co-pyrolysis with plastic. *Fuel, 285*, 119188. https://doi.org/10.1016/j.fuel.2020.119188

Armada, D., Llompart, M., Celeiro, M., Garcia-Castro, P., Ratola, N., Dagnac, T., & de Boer, J. (2022). Global evaluation of the chemical hazard of recycled tire crumb rubber employed on worldwide synthetic turf football pitches. *Science of The Total Environment, 812*, 152542. https://doi.org/10.1016/j.scitotenv.2021.152542

Balogun, A. O., Adeleke, A. A., Ikubanni, P. P., Adegoke, S. O., Alayat, A. M., & Mcdonald, A. G. (2021). Kinetics modeling, thermodynamics and thermal performance assessments of pyrolytic decomposition of moringa oleifera husk and delonix regia pod. *Scientific Reports, 11*, 13862. https://doi.org/10.1038/s41598-021-93407-1

Criado, J. M., Málek, J., & Ortega, A. (1989). Applicability of the master plots in kinetic analysis of non-isothermal data. *Thermochimica Acta, 147*, 377-385. https://doi.org/10.1016/0040-6031(89)85192-5

Danon, B., Mkhize, N. M., Van Der Gryp, P., & Görgens, J. F. (2015). Combined model-free and model-based devolatilisation kinetics of tyre rubbers. *Thermochimica Acta, 601*, 45-53. https://doi.org/10.1016/j.tca.2014.12.003

Doyle, C.D. (1965). Series approximations to the equation of thermogravimetric data. *Nature Publishing Group, 207*, 290-291. https://doi.org/10.1038/207290a0

Dziemidkiewicz, A., Maciejewska, M., & Pingot, M. (2019). Thermal analysis of halogenated rubber cured with a new cross-linking system. *Journal of Thermal Analysis and Calorimetry, 138*, 4395-4405. https://doi.org/10.1007/s10973-019-08881-7

EPA. (2020). Advancing sustainable materials management: Facts and figure report. *United Sates Environmental Protection Agency*. https://www.epa.gov/facts-and-figures-about-materials-waste-and-recycling/advancing-sustainable-materials-management

Flynn, J. H., & Wall, L. A. (1966). General treatment of the thermogravimetry of polymers. *Journal of Research of the National Bureau of Standards–A Physics and Chemistry, 70A*, 487-523. https://doi.org/10.1080/00048407212341221

Friedman, H. L. (1964). Kinetics of thermal degradation of char-forming plastics from thermogravimetry. *Application to a phenolic plastic. Journal of Polymer Science Part C: Polymer Symposia, 6*, 183-195. https://doi.org/10.1002/polc.5070060121

Han, J., Li, W., Liu, D., Qin, L., Chen, W., & Xing, F. (2018). Pyrolysis characteristic and mechanism of waste tyre: A thermogravimetry-mass spectrometry analysis. *Journal of Analytical and Applied Pyrolysis, 129*, 1-5. https://doi.org/10.1016/j.jaap.2017.12.016

He, Q., Ding, L., Gong, Y., Li, W., Wei, J., & Yu, G. (2019). Effect of torrefaction on pinewood pyrolysis kinetics and thermal behavior using thermogravimetric analysis. *Bioresource Technology, 280*, 104-111. https://doi.org/10.1016/j.biortech.2019.01.138

Huang, Y. W., Chen, M. Q., & Li, Y. (2017). An innovative evaluation method for kinetic parameters in distributed activation energy model and its application in thermochemical process of solid fuels. *Thermochimica Acta, 655*, 42-51. https://doi.org/10.1016/j.tca.2017.06.009

Irmak Aslan, D., Parthasarathy, P., Goldfarb, J. L., & Ceylan, S. (2017). Pyrolysis reaction models of waste tires: Application of master-plots method for energy conversion via devolatilization. *Waste Management, 68*, 405-411. https://doi.org/10.1016/j.wasman.2017.06.006

Kawale, H. D., & Kishore, N. (2021). Thermochemical putrefaction of delonix regia biomass and tube waste to produce high-quality pyrolytic bio-oil. *Journal of Thermal Analysis and Calorimetry, 147*, 2969-2983. https://doi.org/10.1007/s10973-021-10725-2

Khiari, B., Kordoghli, S., Mihoubi, D., Zagrouba, F., & Tazerout, M. (2018). Modeling kinetics and transport phenomena during multi-stage tire wastes pyrolysis using Comsol®. *Waste Management, 78*, 337-345. https://doi.org/10.1016/j.wasman.2018.06.002

Kishore, N., Sachan, S., Rai, K. N., & Kumar, A. (2003). Synthesis and characterization of a nanofiltration carbon membrane derived from phenol-formaldehyde resin. *Carbon, 41*, 2961-2972. https://doi.org/10.1016/S0008-6223(03)00427-5

Kordoghli, S., Khiari, B., Paraschiv, M., Zagrouba, F., & Tazerout, M. (2017a). Impact of different catalysis supported by oyster shells on the pyrolysis of tyre wastes in a single and a double fixed bed reactor. *Waste Management, 67*, 288-297. https://doi.org/10.1016/j.wasman.2017.06.001

Kordoghli, S., Paraschiv, M., Kuncser, R., Tazerout, M., & Zagrouba, F. (2017b). Catalysts' influence on thermochemical decomposition of waste tires. *Environmental Progress and Sustainable Energy, 36*, 1560-1567. https://doi.org/10.1002/ep.12605

Labaki, M., & Jeguirim, M. (2017). Thermochemical conversion of waste tyres–a review. *Environmental Science and Pollution Research, 24*, 9962-9992. https://doi.org/10.1007/s11356-016-7780-0

Lah, B., Klinar, D., & Likozar, B. (2013). Pyrolysis of natural, butadiene, styrene-butadiene rubber and tyre components: Modelling kinetics and transport phenomena at different heating rates and formulations. *Chemical Engineering Science, 87*, 1-13. https://doi.org/10.1016/j.ces.2012.10.003

Miura, K., & Maki, T. (1998). A simple method for estimating f(E) and k_0(E) in the distributed activation energy model. *Energy and Fuels, 12*(5), 864-869. https://doi.org/10.1021/ef970212q

Neves, R. M., Ornaghi, H. L., Ornaghi, F. G., Amico, S. C., & Zattera, A. J. (2022). Degradation kinetics and lifetime prediction for polystyrene/nanocellulose nanocomposites. *Journal of Thermal Analysis and Calorimetry, 147*, 879-890. https://doi.org/10.1007/s10973-020-10316-7

Nikiema, J., & Asiedu, Z. (2022). A review of the cost and effectiveness of solutions to address plastic pollution. *Environmental Science and Pollution Research, 29*, 24547-24573. https://doi.org/10.1007/s11356-021-18038-5

Nkosi, N., Muzenda, E., Gorimbo, J., & Belaid, M. (2021). Developments in waste tyre thermochemical conversion processes: Gasification, pyrolysis and liquefaction. *RSC Advances, 11*, 11844-11871. https://doi.org/10.1039/d0ra08966d

Ozawa, T. (1965). A new method of analyzing thermogravimetric data. *Bulletin of the Chemical Society of Japan, 38*, 1881-1886. https://doi.org/10.1246/bcsj.38.1881

Peñalver, R., Costa-Gómez, I., Arroyo-Manzanares, N., Moreno, J. M., López-García, I., Moreno-Grau, S., & Cordoba, M. H. (2021). Assessing the level of airborne polystyrene microplastics using thermogravimetry-mass spectrometry: Results for an agricultural area. *Science of The Total Environment, 787*, 147656. https://doi.org/10.1016/j.scitotenv.2021.147656

Pradhan, D., & Singh, R. K. (2015). Characterization of the liquid product obtained by the pyrolysis of a bicycle tube. *Energy Sources, Part A: Recovery, Utilization and Environmental Effects, 37*, 2099-2106. https://doi.org/10.1080/15567036.2011.608106

Qiu, T., Ge, F., Li, C., & Lu, S. (2022). Study of the thermal degradation of flame-retardant polyester GFRP using TGA and TG-FTIR-GC/MS. *Journal of Thermal Analysis and Calorimetry, 147*, 5743-5760. https://doi.org/10.1007/s10973-021-10895-z

Qu, B., Li, A., Qu, Y., Wang, T., Zhang, Y., Wang, X., Gao, Y., Fu, W., & Ji, G. (2020). Kinetic analysis of waste tire pyrolysis with metal oxide and zeolitic catalysts. *Journal of Analytical and Applied Pyrolysis, 152*, 104949. https://doi.org/10.1016/j.jaap.2020.104949

Rammohan, D., Kishore, N., & Uppaluri, R. V. S. (2022a). Insights on kinetic triplets and thermodynamic analysis of delonix regia biomass pyrolysis. *Bioresource Technology, 358*, 127375. https://doi.org/10.1016/j.biortech.2022.127375

Rammohan, D., Kishore, N., & Uppaluri, R. V. S. (2022b). Reaction kinetics and thermodynamic analysis of non-isothermal co-pyrolysis of Delonix regia and tube waste. *Bioresource Technology Reports, 18*, 101032. https://doi.org/10.1016/j.biteb.2022.101032

Shimada, K., Ikeda, R., Kikura, H., & Takahashi, H. (2020). Enhancement of diversity in production and application utilizing electrolytically polymerized rubber sensors with MCF: 1st report on consummate fabrication combining varied kinds of constituents with porous permeant stocking-like rubber. *Sensors (Switzerland), 20*, 1-26. https://doi.org/10.3390/s20174658

Sibeko, M. A., Adeniji, A. O., Okoh, O. O., & Hlangothi, S. P. (2020). Trends in the management of waste tyres and recent experimental approaches in the analysis of polycyclic aromatic hydrocarbons (PAHs) from rubber crumbs. *Environmental Science and Pollution Research, 27*, 43553-43568.https://doi.org/10.1007/s11356-020-09703-2

Singh, G., Varma, A. K., Almas, S., Jana, A., Mondal, P., & Seay, J. (2019). Pyrolysis kinetic study of waste milk packets using thermogravimetric analysis and product characterization. *Journal of Material Cycles and Waste Management, 21*, 1350-1360. https://doi.org/10.1007/s10163-019-00891-9

Singh, S., Patil, T., Tekade, S. P., Gawande, M. B., & Sawarkar, A. N. (2021). Studies on individual pyrolysis and co-pyrolysis of corn cob and polyethylene: Thermal degradation behavior, possible synergism, kinetics, and thermodynamic analysis. *Science of The Total Environment, 783*, 147004. https://doi.org/10.1016/j.scitotenv.2021.147004

Starink, M. J. (2003). The determination of activation energy from linear heating rate experiments: A comparison of the accuracy of isoconversion methods. *Thermochimica Acta, 404*, 163-176. https://doi.org/10.1016/S0040-6031(03)00144-8

Taylor, R. (2020). *Case study cycling industry*. https://www.aston.ac.uk/research/eps/ebri/case-studies/velorim

Vo, T. K., Ly, H. V., Lee, O. K., Lee, E. Y., Kim, C. H., Seo, J.-W., Kim, J., & Kim, S.-S. (2017). Pyrolysis characteristics and kinetics of microalgal aurantiochytrium sp. KRS101. *Energy, 118*, 369-376. https://doi.org/10.1016/j.energy.2016.12.040

Volli, V., Gollakota, A. R. K., & Shu, C. M. (2021). Comparative studies on thermochemical behavior and kinetics of lignocellulosic biomass residues using TG-FTIR and Py-GC/MS. *Science of The Total Environment, 792*, 148392. https://doi.org/10.1016/j.scitotenv.2021.148392

Vyazovkin, S., Burnham, A. K., Criado, J. M., Pérez-Maqueda, L. A., Popescu, C., & Sbirrazzuoli, N. (2011). ICTAC Kinetics Committee recommendations for performing kinetic computations on thermal analysis data. *Thermochimica Acta, 520*(1-2), 1-19. https://doi.org/10.1016/j.tca.2011.03.034

Wang, B., Fu, Y., Zheng, H., Zeng, D., & Xiao, R. (2021). Catalytic and noncatalytic fast pyrolysis of waste tires to produce high-value monocyclic aromatic hydrocarbons. *Journal of Analytical and Applied Pyrolysis, 156*, 105131. https://doi.org/10.1016/j.jaap.2021.105131

Wen, S., Yan, Y., Liu, J., Buyukada, M., & Evrendilek, F. (2019). Pyrolysis performance, kinetic, thermodynamic, product and joint optimization analyses of incense sticks in N_2 and CO_2 atmospheres. *Renewable Energy, 141*, 814-827. https://doi.org/10.1016/j.renene.2019.04.040

Xu, F., Wang, B., Yang, D., Ming, X., Jiang, Y., Hao, J., Qiao, Y., & Tian, Y. (2018). TG-FTIR and Py-GC/MS study on pyrolysis mechanism and products distribution of waste bicycle tire. *Energy Conversion and Management, 175*, 288-297. https://doi.org/10.1016/j.enconman.2018.09.013

Xu, J., Yu, J., He, W., Huang, J., Xu, J., & Li, G. (2021). Replacing commercial carbon black by pyrolytic residue from waste tire for tire processing: Technically feasible and economically reasonable. *Science of The Total Environment, 793*, 148597. https://doi.org/10.1016/j.scitotenv.2021.148597

Xu, J., Yu, J., Xu, J., Sun, C., He, W., Huang, J., & Li, G. (2020). High-value utilization of waste tires: A review with focus on modified carbon black from pyrolysis. *Science of The Total Environment, 742*, 140235. https://doi.org/10.1016/j.scitotenv.2020.140235

Youn, J.-S., Kim, Y.-M., Siddiqui, M. Z., Watanabe, A., Han, S., Jeong, S., Jung, Y.-W., & Jeon, K.-J. (2021). Quantification of tire wear particles in road dust from industrial and residential areas in Seoul, Korea. *Science of the Total Environment, 784*, 147177. https://doi.org/10.1016/j.scitotenv.2021.147177

Yurdakul, S., Gurel, B., Varol, M., Gurbuz, H., & Kurtulus, K. (2021). Investigation on thermal degradation kinetics and mechanisms of chicken manure, lignite, and their blends by TGA. *Environmental Science and Pollution Research, 28*, 63894-63904.https://doi.org/10.1007/s11356-021-12732-0